CrystEngComm

PAPER

View Article Online
View Journal | View Issue

Cite this: *CrystEngComm*, 2018, **20**, 7486

Controlled synthesis of Fe_3O_4@ZIF-8 nanoparticles for drug delivery†

Guihuan Chen,[a] Bing Yu,[ab] Chenghao Lu,[a] Haohao Zhang,[a] Youqing Shen[ac] and Hailin Cong *[ab]

Received 4th August 2018,
Accepted 8th October 2018

DOI: 10.1039/c8ce01302k

rsc.li/crystengcomm

Encapsulating well-defined nanoparticles (NPs) into ZIF-8 to form core–shell structures not only can minimize the drawbacks and maximize the advantages of the disparate components but also may provide synergistic functionality. This work presents novel one-pot synthetic methods to produce Fe_3O_4@ZIF-8 NPs. Moreover, the morphology of Fe_3O_4@ZIF-8 NPs can be easily controlled by changing the synthesis conditions (time, temperature, and dosage). The as-obtained Fe_3O_4@ZIF-8 NPs have good dispersibility and a large specific surface area and they are proven to have potential applications as drug delivery models with good biocompatibility, high drug loading and good pH responsiveness.

Introduction

In the past decades, a great deal of interest has been devoted to metal–organic framework (MOF) materials due to their adjustable pore size, high pore volume, high specific surface area and highly ordered crystalline porous network characteristics.[1–3] Since the 1990s,[4] they have been widely used in areas such as gas storage,[5,6] separation,[7] catalysis,[8] drug delivery,[9] imaging,[9] sensing[10] and light-harvesting.[11] Under relatively mild conditions, MOFs of crystalline or amorphous materials can be obtained. Their synthesis methods are much simpler and more efficient than those of typical inorganic porous materials (such as silica).[12] As is known, the properties of nanomaterials can be influenced by their composition, size and morphology.[10] So far, the application of MOF materials is still far from enough and needs to be further explored and developed.

To date, the fabrication of multicomponent nanostructured hybrids, which are combined with several different kinds of materials with varied functionalities, has gained wide attention.[13] In recent years, more and more MOF-based composite materials have been synthesized.[14–17] Combining the porous properties of MOF materials with magnetic properties, materials for use in catalytic magnetic separation,[18] magnetic resonance,[19] drug delivery,[20] imaging[21] and other areas of potential application have been explored. A zeolite imidazolate framework (ZIF) is an important metal–organic framework (MOF), which has been attracting more and more attention in the past decades.[22] ZIF possesses a zeolite topology in which divalent metal cations are linked to a tetrahedral framework by imidazole acid anions, resulting in a large surface area and pore volume and unique inherent biodegradability.[23] Lu *et al.* prepared multi-core Fe_3O_4@ZIF-8 with PVP-stabilized 8 nm Fe_3O_4 NPs.[24] Bian *et al.* developed Fe_3O_4@PAA/AuNCs/ZIF-8 NPs with CTAB-modified Fe_3O_4.[25] Previously, the preparation process required additional modification of the prepared iron oxide nanoparticles to further coat ZIF-8. In addition, CTAB has been shown to be cytotoxic in previous studies.[26] In addition, the procedure was time-consuming and involved multiple steps. This motivates us to explore a simple and fast method to synthesize Fe_3O_4@ZIF-8.

In this work, we developed and studied a simple strategy for the synthesis of ZIF-8-coated Fe_3O_4 and studied their physical properties such as their morphology, specific surface area and pH responsiveness as an anticancer drug carrier. We prepared sodium citrate-modified iron oxide with a particle size of 120 nm with good hydrophilicity and excellent dispersion. The three carboxyl groups of Na_3Cit have a strong affinity for Fe^{III} and they favor the attachment of citrate groups on the surface of magnetite nanocrystals which prevents them from being previously aggregated into large single crystals.[27] Na_3Cit is widely used as a surfactant in the preparation of various metal nanoparticles. In addition, Na_3Cit is widely used in the food and pharmaceutical industries and it is one of the products of the human body's normal metabolic

[a] *Institute of Biomedical Materials and Engineering, College of Materials Science and Engineering, College of Chemistry and Chemical Engineering, Qingdao University, Qingdao 266071, China. E-mail: conghailin@qdu.edu.cn; Tel: +86 532 8595 3995*
[b] *Laboratory for New Fiber Materials and Modern Textile, Growing Base for State Key Laboratory, Qingdao University, Qingdao 266071, China*
[c] *Key Laboratory of Biomass Chemical Engineering of Ministry of Education, Center for Bionanoengineering and Department of Chemical and Biological Engineering, Zhejiang University, Hangzhou, Zhejiang, 310027, China*

† Electronic supplementary information (ESI) available. See DOI: 10.1039/c8ce01302k

processes.[28] As far as we know, there is no report about using sodium citrate-modified ferric oxide to prepare Fe_3O_4@ZIF-8 with different morphologies under different conditions. Furthermore, DOX as a model drug was used to confirm the drug loading and pH-sensitive release of Fe_3O_4@ZIF-8 NPs (180 nm) which could be employed as drug carriers *in vitro*.

Materials and methods

Materials

The following provides information on the chemicals used in this work: 2-methylimidazole (2-MeIM) (Aldrich, 99.0%), zinc nitrate hexahydrate ($Zn(NO_3)_2{\cdot}6H_2O$, Sigma-Aldrich, ≥99.0%), sodium citrate (99%), iron trichloride (99%), ethylene glycol and methanol were obtained from Aladdin Reagent Company (Shanghai, China).

Preparation of Fe_3O_4

In a normal procedure, Fe_3O_4 NPs were prepared by a solvothermal method[29] as follows: 1.14 g $FeCl_3{\cdot}6H_2O$ and 2.4 g sodium acetate with 0.65 g sodium citrate were dissolved in 50 ml ethylene glycol and magnetically stirred for 30 min at room temperature. Then the solution was transferred to a Teflon-sealed autoclave and heated at 200 °C for 10 h. Fe_3O_4NPs with a size of 120 nm were separated with a magnet and washed with deionized water and methanol. Finally, the NPs were dried under vacuum at ambient temperature.

Preparation of Fe_3O_4@ZIF-8 core–shell nanostructures

In a normal procedure, Fe_3O_4 NP solution (4 mL, 0.25 mg mL^{-1}) was added to a solution of HMeIM in methanol (26 mL, 0.82 g). The solution was ultrasonicated for 15 min, and 10 mL of $Zn(NO_3)_2$ in methanol (30 mM) was added and allowed to react at room temperature for 2 h without stirring. Finally, the product was separated using a magnet and washed with methanol.

Drug loading of Fe_3O_4@ZIF-8 NPs

In order to determine the encapsulation efficiency, several DOX aqueous solutions in the concentration range of 0–75 μg mL^{-1} were prepared to obtain a calibration curve. The absorbance of DOX remaining in the solvent was measured at the wavelength of its maximum absorbance (λ_{Max} = 480 nm) by UV-vis and then calculated based on the calibration curve. The amount of DOX not loaded in the supernatant was also measured using a UV-vis spectrophotometer (480 nm). The amount of drug loaded, as a measure of the drug load capacity of an important parameter, can be calculated by the following equation: load efficiency (%) = $(m_1 - m_2)/m$, where m_1, m_2 and m represent the initial weight of DOX, the weight of DOX present in the excess solvent and the weight of hollow ZIF-8.

Drug release from DOX-loaded NPs

5 mg drug-loaded nanoparticles (DOX-loaded Fe_3O_4@ZIF-8) were dispersed in 5 ml buffer solution of pH = 7.4 and pH = 5.5, and the drug was released by shaking at 37 °C. At the same time interval, the supernatants of each group were collected by magnetic separation and the amount of DOX released therein was measured with a UV-visible spectrophotometer. Then, 5 ml of fresh PBS solution was added to the release system to continue the drug release process.

Magnet-targeted photothermal effect

2.0×10^5 HeLa cells were incubated in a cell culture dish containing 2 ml of cell culture medium for 24 hours. Then the original cell culture medium was replaced by 4 mg ml^{-1} Fe3O4@ZIF-8 solution which was prepared with culture medium and incubated for another 3 hours. The Fe_3O_4@ZIF-8 NPs were drawn to the specified area of the cell culture dish with a magnet, then all the cells were irradiated by an 808 nm laser with a power density of 2.5 W cm^{-2} for 600 s. After incubation for 3 h, all the cells were stained with calcein-AM and PI solution and the survival rate was observed using a fluorescence inverted microscope (Olympus).

Material characterization

The Fe_3O_4@ZIF-8 NPs were investigated by scanning electron microscopy (SEM, JEOL JSM-6309LV) and transmission electron microscopy (TEM, JEOL JEM-1200). Fourier transform infrared spectroscopy (FT-IR) was performed on a Tensor 27 produced by Bruker Corporation. The powder X-ray diffraction (XRD) patterns of the Fe_3O_4 and Fe_3O_4@ZIF-8 microspheres were recorded on an Ultima IV (185 mm) diffractometer with a Cu target (40 kV/40 mA) from 5° to 90°. Magnetic measurements of the magnetic microspheres were carried out on an alternating gradient magnetometer (Micro Mag TM 2900) at room temperature. The magnetic field was created by a superconducting solenoid in persistent mode. The average hydrodynamic particle size of the Fe_3O_4 and Fe_3O_4@ZIF-8 NPs were determined by dynamic light scattering (DLS) using a Microtrac at 25 °C. UV-vis absorption experiments using a Shimadzu 220 V (E) UV-vis spectrophotometer were carried out to determine the concentration of DOX.

Results and discussion

The preparation of Fe_3O_4@ZIF-8 NPs was carried out using the strategy illustrated in Scheme 1. The magnetic Fe_3O_4 particles were first prepared from $FeCl_3{\cdot}6H_2O$ with sodium acetate (NaAC) and Na_3Cit as stabilizers and ethylene glycol as a reducing agent in a solvothermal reaction. Then, the Fe_3O_4@ZIF-8 composite was synthesized by *in situ* self-assembly of ZIF-8 on the Fe_3O_4 surface to obtain the core–shell structure. The developed approach avoids time-consuming MOF growth and further modification of core particles, which is much simpler than most methods of synthesizing MOF-based core–shell composites.[24,25] In addition,

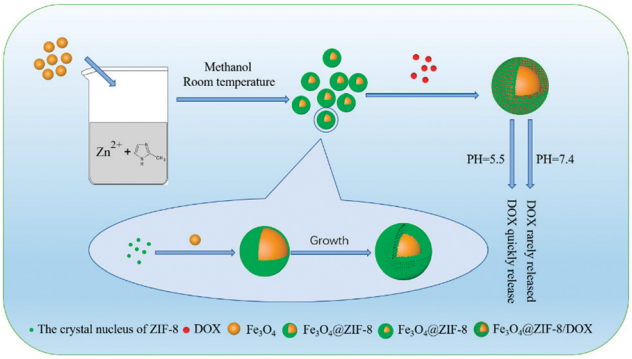

Scheme 1 Schematic illustration of Fe_3O_4@ZIF-8 particle synthesis.

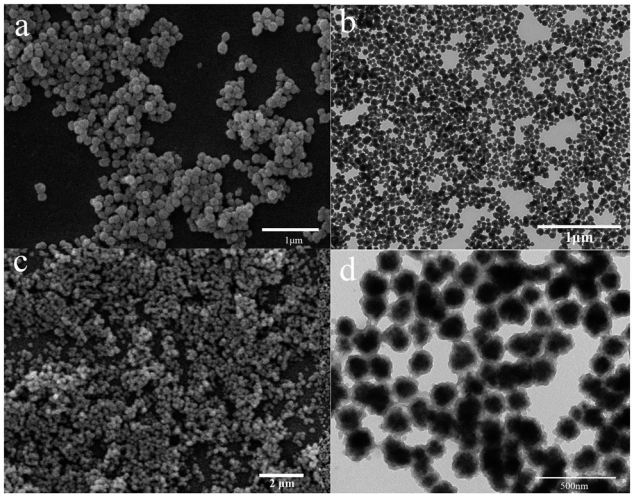

Fig. 1 SEM of Fe_3O_4 (a) and SCS-1 (c). TEM of Fe_3O_4 (b) and SCS-1 (d).

avoiding toxic surface modification makes the as-synthesized Fe_3O_4@ZIF-8 NPs more biocompatible for further biological applications. The synthesized single core–shell structures are denoted as SCS-*x*, where *x* refers to different reaction conditions, as indicated in Table 1.

The structure and morphology of Fe_3O_4 and Fe_3O_4@ZIF-8(SCS-1) were characterized by SEM, TEM (Fig. 1) and DLS (Fig. S1 and S2†). The SEM and DLS results (Fig. 1a, S1 and S2†) show that the prepared Fe_3O_4 (120 nm) and Fe_3O_4@ZIF-8 (180 nm) NPs have good dispersivities. The TEM (Fig. 1b and d) images show that the obtained NPs have a single core–shell structure and the shell thickness is 20 ± 5 nm. The zeta potential was determined to study the charged properties which can prove the *in situ* self-assembly of ZIF-8 on Fe_3O_4. For the synthesis of core–shell nanoparticles with ZIF-8 shells, surface modifications (*e.g.*, PVP and CTAB) on the cores are typically required to stabilize the bare cores and increase their affinities to MOF precursors.[30] However, this is not needed for encapsulating Fe_3O_4 NPs as they are negatively charged (Fig. 2a) and have an excellent affinity to zinc ions. The XRD analysis further demonstrates the encapsulation of Fe_3O_4 in ZIF-8. The Fe_3O_4@ZIF-8 particles show a similar XRD pattern compared with the JCPDS file of Fe_3O_4, indicating that the Fe_3O_4 crystal structure does not change after coating with ZIF-8 (Fig. 2d).

The nucleation process of MOFs can be regulated by adjusting the reaction parameters, including the reaction time, temperature and concentration, to obtain different sizes of products.[31] Previous reports suggested that mixing would lead to secondary nucleation of MOFs, resulting in excessive size, so the experiment was kept static. The encapsulation process was further investigated by changing the concentration of Fe_3O_4 and changing the reaction time or reaction temperature (Fig. 3). When the concentration of Fe_3O_4 was increased from 10 to 20 mg, the dispersion worsened, while the shell thickness remained unchanged. As the concentration of Fe_3O_4 was decreased from 10 to 1 mg, the shell thickness remained unchanged. Excess HMeIM may not only act as a base for the deprotonation of the bridging ligands but also as a capping agent capable of inhibiting ZIF-8 crystalline growth.[32] As the concentration of Fe_3O_4 was increased, the massive consumption of HMeIM caused the dispersion to worsen. In contrast, there was excess HMeIM when the concentration of Fe_3O_4 was decreased which may enhance the stability of the solution. However, thick-shell structures with a uniform size and shape were obtained when the reaction time was increased from 1 to 2 h. When the reaction temperature was 4 °C, the Fe_3O_4 NPs were encapsulated in the ZIF-8 crystals as well. It can be seen from the TEM images (Fig. 3b–d) that there are two different structures obtained. This can be explained by the rate of nucleation being dependent on the synthesis temperature. A faster nucleation at a high synthesis temperature leads to a higher concentration of nanoparticles. At a low temperature, the nucleation is slowed down. This results in fewer nucleating particles which can grow larger in the presence of abundant starting materials.[33]

The FTIR spectra of the synthesized citrate-capped Fe_3O_4 NPs and the core–shell structure of the Fe_3O_4@ZIF-8 NPs are illustrated in Fig. 4a. SCS-1, SCS-2 and SCS-5 in Fig. 4a exhibited strong IR absorption in the low-frequency region

Table 1 SCS-*x*

SCS-*x*	$Zn(NO_3)_2$/mg	HMeIM/mg	Fe_3O_4/mg	Time/min	Temperature/°C
x = 1	372	820	10	60	25
x = 2	372	820	10	120	25
x = 3	372	820	1	60	25
x = 4	372	820	20	60	25
x = 5	372	820	10	60	4

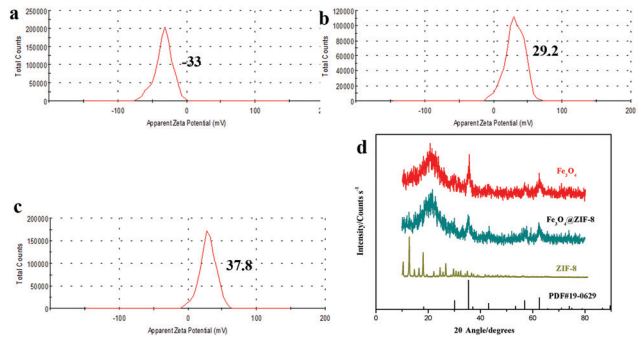

Fig. 2 Zeta potential of Fe_3O_4 (a), SCS-1 (b) and ZIF-8 (c). XRD of Fe_3O_4, SCS-1 and ZIF-8 (d).

due to the Fe–O skeleton of the Fe_3O_4 nanoparticles. Meanwhile in bulk magnetite, the Fe–O stretching band appears at 375 cm^{-1}, due to the quantum confinement effects of Fe_3O_4 nanoparticles, and it was shifted to 580 cm^{-1} in the case of Fe_3O_4 nanoparticles.[34] The characteristic stretching vibration peaks of the carboxyl groups in the SCS-1, SCS-2 and SCS-5 samples are relatively weak compared with those of pure Fe_3O_4 at 1652 and 1396 cm^{-1}. Trisodium citrate dihydrate not only plays an important role in controlling the Fe_3O_4 morphology but also acts as a surface modification agent through the carboxylate groups. The growth of the ZIF-8 shell on the Fe_3O_4 particles can be initiated by Zn^{2+} ions binding to the carboxylate groups on the Fe_3O_4 particle surface. Thereafter, 2-methylimidazole coordinates with the Zn^{2+} ions to form ZIF-8. FTIR spectroscopy was performed to prove the successful coating of ZIF-8. In FTIR spectroscopy, the peaks in the 1100–1400 cm^{-1} region are assigned to the C–N stretching of ZIF-8. There is a characteristic peak at 3426 cm^{-1} of the product, indicating the presence of hydroxyl groups on the surface of Fe_3O_4@ZIF-8 nanoparticles. These hydrophilic groups on the surface of a nanocarrier can attenuate the removal of particles from the reticuloendothelial system (RES) of an organism and excretion from the body, improving the circulation stability of the particles in the blood.[35]

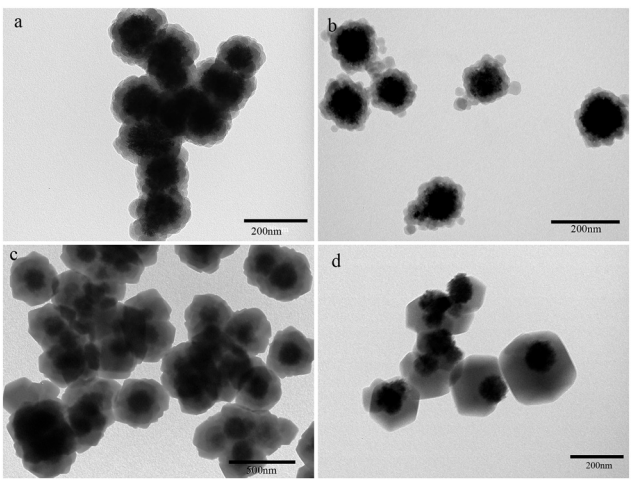

Fig. 3 TEM images of (a) SCS-4, (b) SCS-3, (c) SCS-2 and (d) SCS-5.

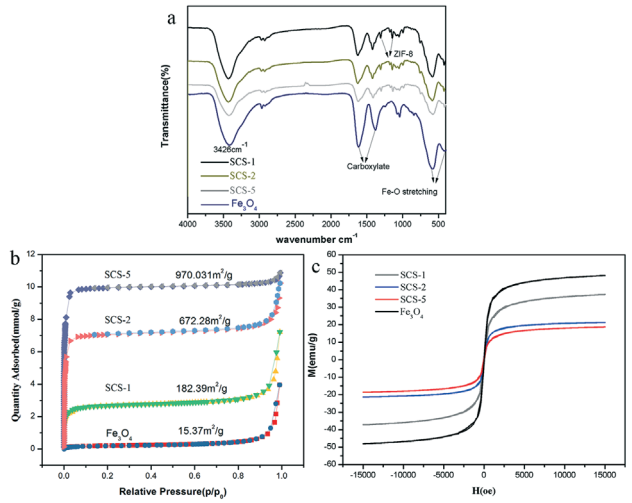

Fig. 4 FT-IR spectra(a), BET(b) and magnetization at 300 K as a function of the applied field (c) of the Fe_3O_4, SCS-1, SCS-2 and SCS-5.

Fig. 4b demonstrates the nitrogen adsorption–desorption isotherm of the Fe_3O_4 nanoparticles, SCS-1, SCS-2 and SCS-5, indicating a type I isotherm. The BET surface area of SCS-1, SCS-2 and SCS-5 was 182.39, 672.28 and 970.03 $m^2\ g^{-1}$, respectively, which is much lower than that of pure ZIF-8 (1570 $m^2\ g^{-1}$) mainly due to the Fe_3O_4 cores.[36] Fig. 4c shows that the Fe_3O_4 nanoparticles, SCS-1, SCS-2 and SCS-5 are superparamagnetic at room temperature. The saturation magnetization (Ms) values of the Fe_3O_4 nanoparticles, SCS-1, SCS-2 and SCS-5 were determined to be 48.1, 37.2, 21.3 and 18.6 emu g^{-1}, respectively. The superparamagnetism and the high Ms values allow the products to be used as targeted drug carriers[36,37] and in MR imaging,[38] adsorption[39,40] and many other applications. In consideration of the enhanced permeability and retention (EPR) effects, the size of the carrier used as a drug transport is limited. In our work, we chose Fe_3O_4@ZIF-8 with a size of 180 nm as a drug carrier to test its performance in drug loading and its pH response performance.

In order to assess the drug loading and controlled release behavior of the Fe_3O_4@ZIF-8 NPs, DOX (an anticancer drug) is selected as a model drug. The high loading efficiency of encapsulation of DOX into the Fe_3O_4@ZIF-8 carriers could reach 76.6%, and an extremely high drug loading content was obtained, DOX/Fe_3O_4@ZIF-8 = 330 mg/1 g, which were determined by means of the characteristic DOX absorption peak at 480 nm (Fig. 5a). As can be seen from the SEM images in Fig. S3,† the loading of DOX does not affect the dispersibility of the Fe_3O_4@ZIF-8 NPs. It is revealed that there are two reasons that explain the high loading efficiency: (1) the electrostatic interaction between the negatively charged carboxylic acid groups and positively charged DOX[17] and (2) the coordination bonding of Zn(II)-DOX.[41] The *in vitro* release rate of Fe_3O_4@ZIF-8 can be controlled by varying the pH at 37 °C. In neutral PBS (pH = 7.4), DOX was released in a very slow fashion and the cumulative release of DOX was only about 32.6% even after 48 h at pH = 7.4 (Fig. 5b and c). In

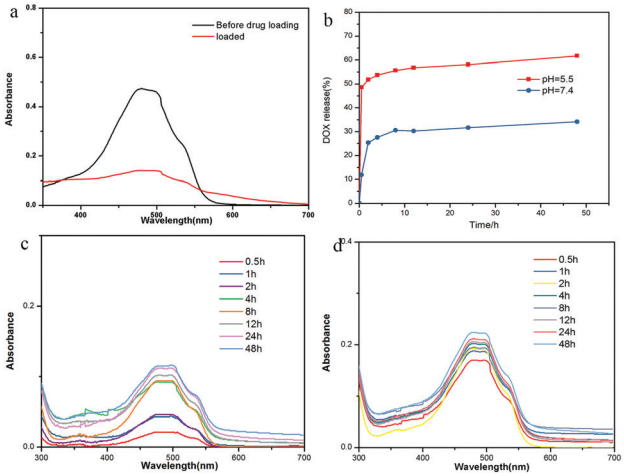

Fig. 5 (a) UV-vis spectra of DOX in the solution before and after drug loading. (b) Time–concentration curves at pH = 5.5 and pH = 7.4. (c) UV-vis spectra of drug release at pH = 7.4 in PBS. (d) UV-vis spectra of drug release at pH = 5.5 in PBS.

contrast, it can be clearly seen that the system shows a faster drug release rate; 63% of DOX was released after 48 h at pH = 5.5 (Fig. 5b and d). Thus, the pH-dependent drug-releasing Fe_3O_4@ZIF-8 system is promising as a drug carrier and is beneficial for targeting cancerous tissues, since the extracellular pH of tumors is lower than that of normal tissues and the microenvironments of tumors are acidic.[3]

In vitro cell viabilities of different concentrations of Fe_3O_4@ZIF-8 and Fe_3O_4 on hepatoma cells were evaluated by MTT assay to study the bio-toxicity of Fe_3O_4@ZIF-8. The Hepatoma cells treated with Fe_3O_4@ZIF-8 showed low toxicity, nearly 80% cell viability even at a concentration of up to 200 mg L^{-1}, indicating the good biocompatibility of the synthesized Fe_3O_4@ZIF-8 composites (Fig. 6). The live–dead staining images of the HeLa cells treated without Fe_3O_4@ZIF-8 solution and those treated with 4 mg ml^{-1} Fe_3O_4@ZIF-8 solution further confirm the low cytotoxicity of Fe_3O_4@ZIF-8 (Fig. S4a and b†). In addition, the magnet-targeted photothermal effect of Fe_3O_4@ZIF-8 was preliminarily investigated here. It is reported that Fe_3O_4 nanoparticles have an excellent photothermal effect in both *in vitro* and *in vivo* experiments under 808 nm laser irradiation.[42] In our experiment, Fe_3O_4@ZIF-8 could be drawn to the specified area of the cell culture dish with a magnet. After treatment with 808 nm laser, the cancer cells were effectively killed in the Fe_3O_4@ZIF-8-enriched area while there was a negligible impact on cancer cells in the Fe_3O_4@ZIF-8-deficient area (Fig. S4c and d†), demonstrating the obvious magnet-targeted property of Fe_3O_4@ZIF-8.

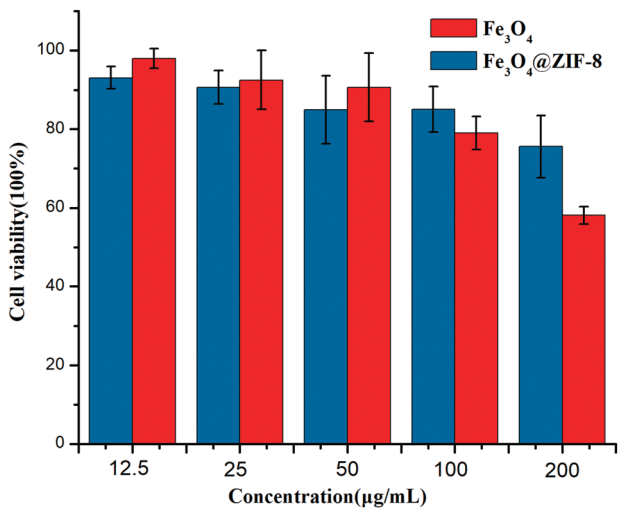

Fig. 6 Cell viability of hepatoma cells after incubation with different concentrations of Fe_3O_4@ZIF-8.

Conclusions

A facile synthetic route has been developed for the preparation of Fe_3O_4@ZIF-8 NP core–shell structures. The growth processes of the nanostructures are carefully investigated, and it is found that the morphology of Fe_3O_4@ZIF-8 NPs can be easily controlled by changing the synthesis conditions (time, temperature, and dosage). The as-obtained Fe_3O_4@ZIF-8 (with size of 180 nm) has good dispersibility and a large specific surface area. The drug loading rate reaches DOX/Fe_3O_4@ZIF-8 = 330 mg g^{-1}. Meanwhile, the drug molecules are effectively controlled from the MOFs at pH = 7.4, and rapid release of the drug can be achieved at pH = 5.5. Our results provide a new route for the synthesis of magnetic MOF-based core–shell materials and shed light on the promising use of Fe_3O_4@ZIF-8 NPs as low-toxicity and biocompatible drug delivery carriers.

Author contributions

Guihuan Chen and Bing Yu contributed equally to this paper.

Conflicts of interest

There are no conflicts to declare.

Acknowledgements

This work is financially supported by the National Natural Science Foundation of China (21675091, 21574072, and 21874078), the Taishan Young Scholar Program of Shandong Province (tsqn20161027), the Major Science and Technology Innovation Project of Shandong Province (2018CXGC1407), the Key Research and Development Project of Shandong Province (2016GGX102028, 2016GGX102039, and 2017GGX20111), the Natural Science Foundation of Shandong Province (ZR2017BB003), the Postdoctoral Scientific Foundation of China (2017M622126), the Project of Shandong Province Higher Educational Science and Technology Program (J15LC20), the People's Livelihood Science and Technology Project of Qingdao (166257nsh and 173378nsh), the Innovation Leader Project of Qingdao (168325zhc), the Postdoctoral

Scientific Research Foundation of Qingdao, and the First Class Discipline Project of Shandong Province.

Notes and references

1 T. R. Cook, Y. R. Zheng and P. J. Stang, *Chem. Rev.*, 2012, **113**, 734–777.
2 H. Furukawa, K. E. Cordova, M. O'Keeffe and O. M. Yaghi, *Science*, 2013, **341**, 1230444.
3 L. Xing, H. Zheng, Y. Cao and S. Che, *Adv. Mater.*, 2012, **24**, 6433–6437.
4 H. Li, M. Eddaoudi, M. O'Keeffe and O. M. Yaghi, *Nature*, 1999, **402**, 276–279.
5 J. L. C. Rowsell and O. M. Yaghi, *Microporous Mesoporous Mater.*, 2004, **73**, 3–14.
6 R. E. Morris and P. S. Wheatley, *Angew. Chem., Int. Ed.*, 2008, **47**, 4966–4981.
7 J. l. Cao, Y. l. Su, Y. Liu, J. Guan, M. He, R. Zhang and Z. Jiang, *J. Membr. Sci.*, 2018, **566**, 268–277.
8 L. Ma, C. Abney and W. Lin, *Chem. Soc. Rev.*, 2009, **38**, 1248–1256.
9 P. Horcajada, T. Chalati, C. Serre, B. Gillet, C. Sebrie, T. Baati, J. F. Eubank, D. Heurtaux, P. Clayette and C. Kreuz, *Nat. Mater.*, 2010, **9**, 172–178.
10 Z. Xie, L. Ma, K. E. deKrafft, A. Jin and W. Lin, *J. Am. Chem. Soc.*, 2009, **132**, 922–923.
11 C. A. Kent, B. P. Mehl, L. Ma, J. M. Papanikolas, T. J. Meyer and W. Lin, *J. Am. Chem. Soc.*, 2010, **132**, 12767–12769.
12 A. R. Chowdhuri, T. Singh, S. K. Ghosh and S. K. Sahu, *ACS Appl. Mater. Interfaces*, 2016, **8**, 16573–16583.
13 S. Wuttke, S. Braig, T. Preiß, A. Zimpel, J. Sicklinger, C. Bellomo, J. O. Rädler, A. M. Vollmar and T. Bein, *Chem. Commun.*, 2015, **51**, 15752–15755.
14 S. Wang, L. Shang, L. Li, Y. Yu, C. Chi, K. Wang, J. Zhang, R. Shi, H. Shen, G. I. N. Waterhouse, S. Liu, J. Tian, T. Zhang and H. Liu, *Adv. Mater.*, 2016, **28**, 8379–8387.
15 G. Lu, S. Li, Z. Guo, O. K. Farha, B. G. Hauser, X. Qi, Y. Wang, X. Wang, S. Han and X. Liu, *Nat. Chem.*, 2012, **4**, 310–316.
16 L. Chen, Y. Peng, H. Wang, Z. Gu and C. Duan, *Chem. Comun.*, 2014, **50**, 8651–8654.
17 H. Ren, L. Zhang, J. An, T. Wang, L. Li, X. Si, L. He, X. Wu, C. Wang and Z. Su, *Chem. Commun.*, 2014, **50**, 1000–1002.
18 A. Schejn, T. Mazet, V. Falk, L. Balan, L. Aranda, G. Medjahdi and R. Schneider, *Dalton Trans.*, 2015, **44**, 10136–10140.
19 J. Yu, C. Yang, J. Li, Y. Ding, L. Zhang, M. Z. Yousaf, J. Lin, R. Pang, L. Wei and L. Xu, *Adv. Mater.*, 2014, **26**, 4114–4120.
20 K. Deng, Z. Hou, X. Li, C. Li, Y. Zhang, X. Deng, Z. Cheng and J. Lin, *Sci. Rep.*, 2015, **5**, 7851.
21 A. R. Chowdhuri, D. Bhattacharya and S. K. Sahu, *Dalton Trans.*, 2016, **45**, 2963–2973.
22 K. S. Park, Z. Ni, A. P. Côté, J. Y. Choi and R. Huang, *Proc. Natl. Acad. Sci. U. S. A.*, 2006, **103**, 10186–10191.
23 P. Horcajada, R. Gref, T. Baati, P. K. Allan, G. Maurin, P. Couvreur, G. Férey, R. E. Morris and C. Serre, *Chem. Rev.*, 2011, **112**, 1232–1268.
24 G. Lu, S. Li, Z. Guo, O. K. Farha, B. G. Hauser, X. Qi, Y. Wang, X. Wang, S. Han and X. Liu, *Nat. Chem.*, 2012, **4**, 310–316.
25 R. Bian, T. Wang, L. Zhang, L. Li and C. Wang, *Biomater. Sci.*, 2015, **3**, 1270–1278.
26 T. Niidome, M. Yamagata, Y. Okamoto, Y. Akiyama, H. Takahashi, T. Kawano, Y. Katayama and Y. Niidome, *J. Controlled Release*, 2006, **114**, 343–347.
27 H. Deng, X. Li, Q. Peng, X. Wang, J. Chen and Y. Li, *Angew. Chem.*, 2005, **117**, 2842–2845.
28 J. Liu, Z. Sun, Y. Deng, Y. Zou, C. Li, X. Guo, L. Xiong, Y. Gao, F. Li and D. Zhao, *Angew. Chem., Int. Ed.*, 2009, **48**, 5875.
29 J. Liu, Z. Sun, Y. Deng, Y. Zou, C. Li, X. Guo, L. Xiong, Y. Gao, F. Li and D. Zhao, *Angew. Chem., Int. Ed.*, 2009, **48**, 5875–5879.
30 R. Chen, J. Zhang, Y. Wang, X. Chen, J. A. Zapien and C. S. Lee, *Nanoscale*, 2015, **7**, 17299–17305.
31 W. Cai, C. C. Chu, G. Liu and Y. X. Wang, *Small*, 2015, **11**, 4806–4822.
32 J. Cravillon, R. Nayuk, S. Springer, A. Feldhoff, K. Huber and M. Wiebcke, *Chem. Mater.*, 2011, **23**, 2130–2141.
33 C. W. Tsai and E. H. G. Langner, *Microporous Mater.*, 2016, **221**, 8–13.
34 A. Ray Chowdhuri, D. Bhattacharya and S. K. Sahu, *Dalton Trans.*, 2016, **45**, 2963–2973.
35 Y. Pu, S. Chang, H. Yuan, G. Wang, B. He and Z. Gu, *Biomaterials*, 2013, **34**, 3658–3666.
36 X. Yang, X. Zhang, Y. Ma, Y. Huang, Y. Wang and Y. Chen, *J. Mater. Chem.*, 2009, **19**, 2710.
37 A. K. Ebrahimi, M. Barani and I. Sheikhshoaie, *Mater. Sci. Eng., C*, 2018, **92**, 349–355.
38 Y. X. Wang, S. M. Hussain and G. P. Krestin, *Eur. J. Radiol.*, 2001, **11**, 2319–2331.
39 B. Yu, L. He, Y. Wang and H. Cong, *Materials*, 2017, **10**, 1239.
40 B. Yu, B. Yang, G. Li and H. Cong, *J. Mater. Sci.*, 2018, **53**, 6471–6481.
41 H. Zheng, L. Xing, Y. Cao and S. Che, *Coord. Chem. Rev.*, 2013, **257**, 1933–1944.
42 M. Chu, Y. Shao, J. Peng, X. Dai, H. Li, Q. Wu and D. Shi, *Biomaterials*, 2013, **34**, 4078e4088.